

Two-photon photodissociation of H_2O via the $\tilde{\text{B}}$ state

J. Underwood, C. Wittig*

Department of Chemistry, University of Southern California, Los Angeles, CA 90089-0482, USA

Received 23 December 2003

Published online: 7 February 2004

Abstract

The $\text{H}_2\text{O } \tilde{\text{B}} \leftarrow \tilde{\text{X}}$ system has been excited by using 266 nm two-photon absorption, and H-atom products have been probed by using high- n Rydberg time-of-flight spectroscopy. The $\tilde{\text{B}}/\tilde{\text{X}}$ conical intersection results in the efficient transfer of flux from $\tilde{\text{B}}$ to $\tilde{\text{X}}$, with dissociation occurring mainly on $\tilde{\text{X}}$. Though the $\text{OH}(\text{X}^2\Pi)$ product is highly rotationally excited, this bias is less than that observed at higher energies. The $\text{OH}(\text{A}^2\Sigma^+)/\text{OH}(\text{X}^2\Pi)$ branching ratio is $<0.1\%$, which is significantly smaller than branching ratios obtained at higher excitation energies, and two orders of magnitude less than predicted by theory.

© 2004 Published by Elsevier B.V.

1. Introduction

The water molecule, with only 10 electrons, is an ideal system for comparing theory and experiment. Theoretical studies have reproduced with good accuracy the $\tilde{\text{A}}1^1\text{A}'' \leftarrow \tilde{\text{X}}1^1\text{A}'$ absorption spectrum, which is continuous throughout its entire range due to rapid dissociation of the $\tilde{\text{A}}$ state, as well as rovibronic state distributions of the OH product [1,2]. The absorption spectrum and relevant product channels are shown in Fig. 1. Even in the long-wavelength region, where the participation of a triplet state has been invoked, theory has had some, albeit limited, success [3–7].

Whereas, the dynamics of the $\tilde{\text{A}}$ state are relatively simple, involving direct dissociation with little OH rovibronic excitation, the dynamics of the $\tilde{\text{B}}$ state are more complex, as major geometry changes and nonadiabatic effects are involved. A limited number of excitation wavelengths have been examined throughout the $\tilde{\text{B}}2^1\text{A}' \leftarrow \tilde{\text{X}}1^1\text{A}'$ system, whose range lies roughly between 125 and 140 nm. Theoretical predictions are in accord with the room temperature absorption spectrum [8–11] and measured OH rovibronic excitations [11–14]. The $\tilde{\text{B}}$ state involves the promotion of an electron out of the $3a_1$ H–H bonding orbital. This results in a linear

equilibrium geometry with unequal OH bond lengths of 0.95 and 1.6 Å [15]. As used here, the term *equilibrium geometry* refers to the upper sheet of the $\tilde{\text{B}}/\tilde{\text{X}}$ conical intersection. Dissociation that proceeds adiabatically on $\tilde{\text{B}}$ yields $\text{OH}(\text{A}^2\Sigma^+) + \text{H}$.

Seams of $\tilde{\text{B}}/\tilde{\text{X}}$ conical intersection at linear HHO and HOH configurations have been analyzed in detail by Yarkony [16], including derivative couplings. The $\tilde{\text{B}}/\tilde{\text{X}}$ HOH conical intersection, which leads to $\text{OH}(\text{X}^2\Pi) + \text{H}$ with high efficiency, has a dramatic effect on the dynamics of photoinitiated dissociation. Coriolis coupling between the $\tilde{\text{B}}$ and $\tilde{\text{A}}$ Renner–Teller pair near linear geometries can also yield $\text{OH}(\text{X}^2\Pi) + \text{H}$, but this has been shown to be a minor pathway [11].

The OH A/X branching ratio is sensitive to the shape of the $\tilde{\text{B}}$ surface in the region accessed by vertical excitation from the ground state. From this initially accessed region, gradients on the $\tilde{\text{B}}$ surface encourage the system to progress toward products via different mechanisms: adiabatically on $\tilde{\text{B}}$ toward $\text{OH}(\text{A}^2\Sigma^+) + \text{H}$; versus toward the $\tilde{\text{B}}/\tilde{\text{X}}$ conical intersection that results in the efficient production of $\text{OH}(\text{X}^2\Pi) + \text{H}$. The shape of the $\tilde{\text{B}}$ surface in the Franck–Condon region dictates the respective proportions of flux directed along these pathways. Thus, the OH A/X branching ratio can serve as an effective probe of the $\tilde{\text{B}}$ potential surface in the Franck–Condon region.

At all of the excitation energies that have been studied to date in which detection methods sensitive to both

* Corresponding author. Fax: +1-213-740-3972.

E-mail address: wittig@usc.edu (C. Wittig).

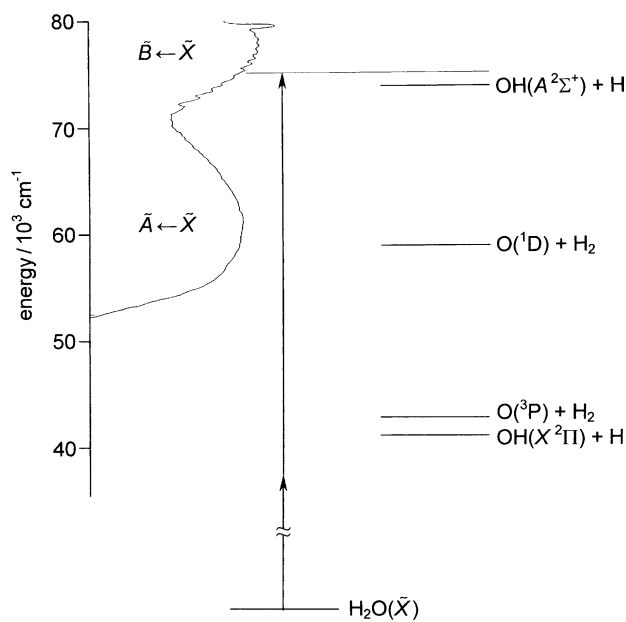


Fig. 1. H_2O absorption spectrum and product energies. Arrows indicate 266 nm two-photon excitation. $D_0(\text{H}-\text{OH})$ is $41\,128\text{ cm}^{-1}$ [26]. The OH X–A energy separation is from [27]. The $\text{O}(^3\text{P}) + \text{H}_2$ and $\text{O}(^1\text{D}) + \text{H}_2$ energies are from [28]. The absorption spectrum is from [29].

$\text{OH}(X^2\Pi)$ and $\text{OH}(A^2\Sigma^+)$ have been used, the major product channel has been found to be $\text{OH}(X^2\Pi) + \text{H}$. This indicates that dissociation occurs primarily on the $\tilde{\text{X}}$ and/or $\tilde{\text{A}}$ surfaces [17–19]. For example, at 121.6 nm, an A/X branching ratio of $\sim 20\%$ has been measured [18,19]. The theoretical study of van Harrevelt and van Hemert [11], yields a branching ratio of $\sim 30\%$ at 121.6 nm, i.e., $\sim 50\%$ higher than the measured value, but they caution that electronic states in addition to $\tilde{\text{B}}$ may be involved at this high energy. At 125.1 nm, Krautwald et al. [17] have estimated a branching ratio of 10% (with theory predicting a ratio of $\sim 20\%$ [11]) by using an H^+ time-of-flight (TOF) method, though they did not account for the $\text{O}(^3\text{P}) + 2\text{H}$ channel, which is energetically accessible in this region.

Accurate OH A/X branching ratios at longer wavelengths in the $\tilde{\text{B}} \leftarrow \tilde{\text{X}}$ system are desirable. It is, practically speaking, not feasible to determine this ratio with acceptable accuracy by using experimental methods that rely on fluorescence from $\text{OH}(A^2\Sigma^+)$ (i.e., emission from nascent $\text{OH}(A^2\Sigma^+)$ and laser induced fluorescence detection of $\text{OH}(X^2\Pi)$), as highly rotationally excited $\text{OH}(A^2\Sigma^+)$ undergoes efficient predissociation. To obtain accurate OH A/X branching ratios, a method is required that is sensitive to high N levels of both $\text{OH}(X)$ and $\text{OH}(A)$. Thus, in the current study, the high- n Rydberg TOF technique has been used to measure the OH A/X branching ratio near the center of the $\tilde{\text{B}} \leftarrow \tilde{\text{X}}$ absorption spectrum.

2. Experimental methods and results

The photodissociation of expansion-cooled H_2O has been examined by using high- n Rydberg time-of-flight (HRTOF) spectroscopy. Measurements of laboratory-frame H-atom translational energy distributions and their conversion to center-of-mass (c.m.) translational energy distributions yield the corresponding OH internal energy distributions. The experimental arrangement is shown in Fig. 2. It has been described in detail elsewhere, and therefore will be discussed here only briefly [20]. A molecular beam containing H_2O is formed by bubbling ~ 760 Torr of argon through H_2O at room temperature, producing a beam of $\sim 3\%$ H_2O . Two-photon photolysis of H_2O is achieved by using 70–80 mJ of 266 nm polarized radiation focused with a 43 cm focal length lens. The polarization of the photolysis radiation is rotated by using a half wave plate. Following photolysis, the nascent H-atoms are probed via HRTOF. A short flight distance of 13.9 cm was used because of low signal-to-noise ratio (S/N).

Fig. 1 indicates the position in the room temperature absorption spectrum that is accessed with two 266 nm photons and the energetically accessible channels. Note that the current study is blind to the $\text{O}(^1\text{D}) + \text{H}_2$ and $\text{O}(^3\text{P}) + \text{H}_2$ channels. The resulting TOF distributions

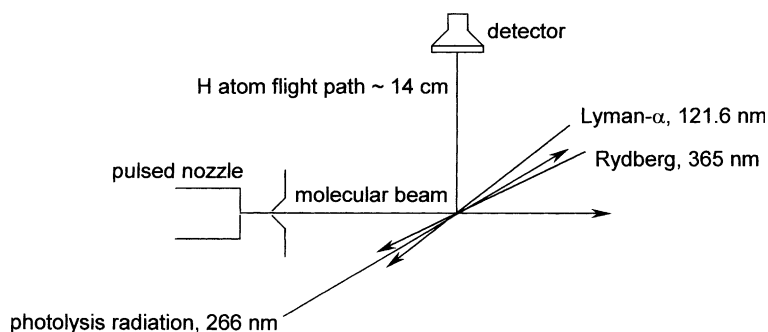


Fig. 2. Schematic of the HRTOF arrangement indicating polarized photodissociation radiation (266 nm) and the radiations used to create high- n Rydberg atoms (121.6 and 365 nm). The flight distance is 13.9 cm.

are shown in Fig. 3a; the spectra represent ~ 5000 laser shots. No products were detected in the region of the $\text{OH}(A^2\Sigma^+) + \text{H}$ channel, even with $\times 50$ magnification. The present work indicates that the $\text{OH}(A)$ channel contributes $<0.1\%$ to the total H-atom signal, whereas theory predicts that $\sim 10\%$ of the products are in the $\text{OH}(A)$ channel at this excitation energy [11]. This negligible contribution from the $\text{OH}(A) + \text{H}$ channel underscores the effectiveness of the $\tilde{\text{B}}/\tilde{\text{X}}$ conical intersection.

Transformations of the TOF spectra to c.m. translational energy distributions yield the OH internal energy distributions shown in Fig. 3b. The weakly structured broad distribution that peaks near 7000 cm^{-1} indicates that the OH has considerable internal excitation. No high energy H-atoms are present. We assign the lumpy peaks to high rotational levels of $\text{OH}(X, v=0)$ superimposed on rotationally excited OH in higher vibrational levels. Resolution of individual rotational

levels of OH is not possible due to the short flight distance used in the current experiment. Previous studies of the $\tilde{\text{B}} \leftarrow \tilde{\text{X}}$ system have observed highly rotationally excited OH with modest vibrational excitation [14,17–19,21–25], and calculations indicate that this type of distribution should dominate throughout the $\tilde{\text{B}} \leftarrow \tilde{\text{X}}$ system [11].

A small degree of spatial anisotropy is observed. This is due to both the direction of the transition dipole moment and the promptness of the dissociation. The $\tilde{\text{B}} \leftarrow \tilde{\text{X}}$ transition dipole moment lies along both the z - and y -axes, due to strong mixing of the $\tilde{\text{B}}$, $\tilde{\text{D}}$, and $\tilde{\text{E}}$ states (the molecule lies in the y - z plane and the z -axis bisects the HOH bond angle). If the molecule is constrained to C_{2v} geometries then $\mu_y = 0$ [15]. In the limit of prompt dissociation and $\mu_y = 0$, the experimental apparatus is more sensitive to products that derive from horizontal photolysis polarization because the mean angle between the transition dipole moment and the

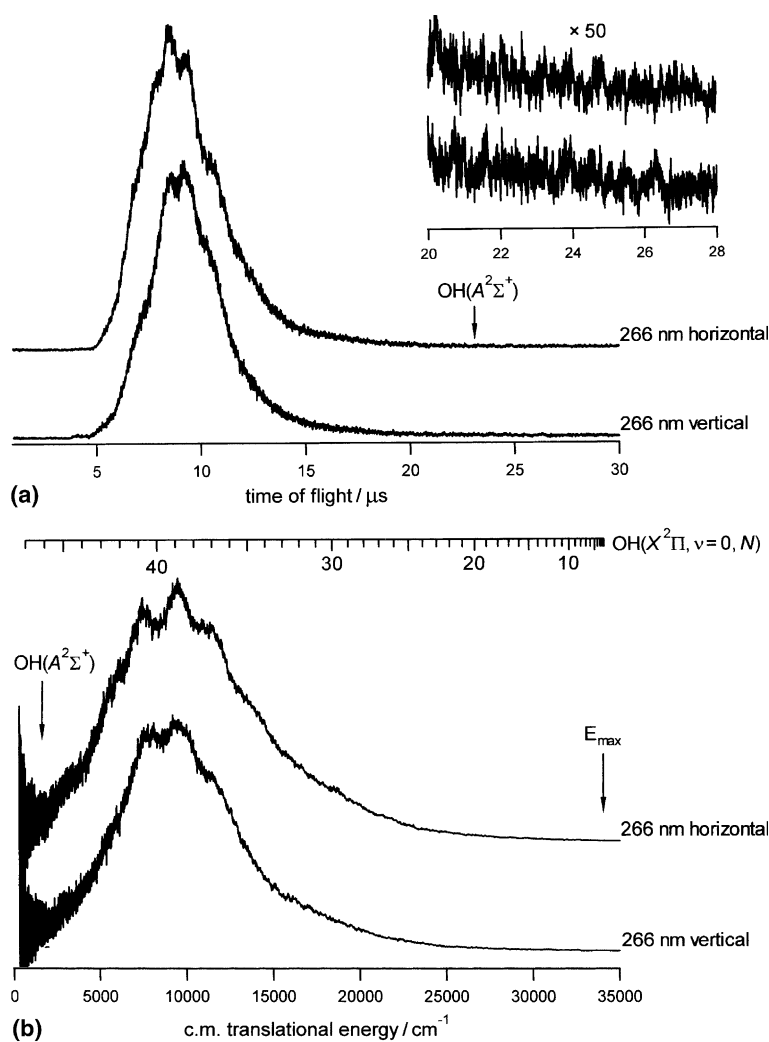


Fig. 3. (a) Time-of-flight distributions. No $\text{OH}(A^2\Sigma^+)$ is detected at $\times 50$ magnification. (b) Center-of-mass translational energy distributions. The broad peak is attributed to highly rotationally excited $\text{OH}(X^2\Pi)$ in $v=0$ with structure due to $v>0$.

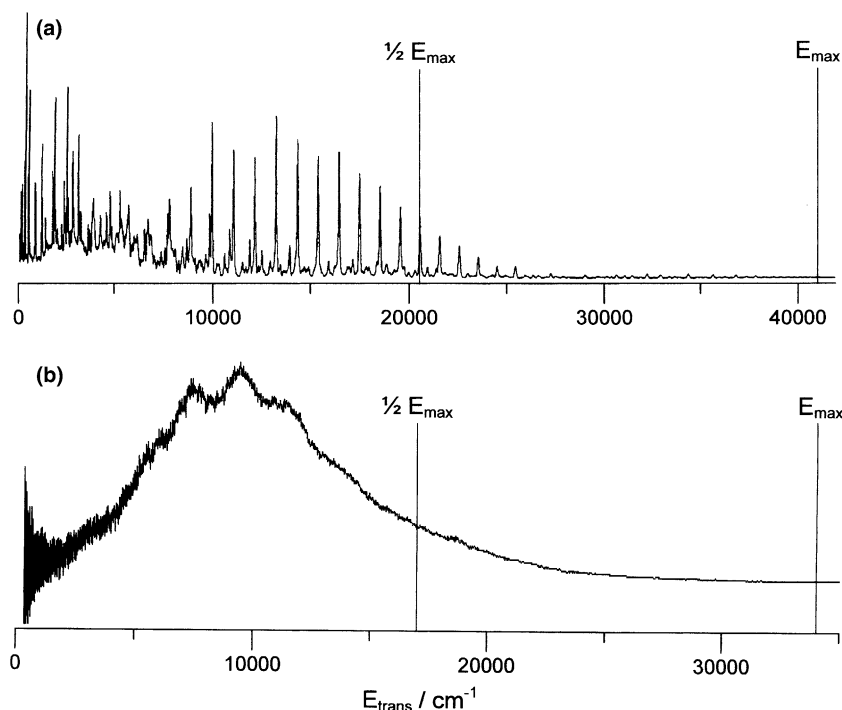


Fig. 4. Translational energy distribution for horizontally polarized photolysis radiation: (a) 121.6 nm, from [18]; (b) this work. Vertical lines indicate the maximum energy and half the maximum energy. There is less bias toward highly rotationally excited OH(X) as the photodissociation energy decreases.

detection axis is less than for vertical polarizations. For $\mu_y \neq 0$, the resulting signal is expected to show modest anisotropy, even in the case of prompt dissociation.

Fig. 4a shows the HRTOF results of Harich et al. [19] obtained by using horizontally polarized 121.6 nm photolysis radiation. Despite their higher resolution and better S/N, a valuable comparison with the present study can be made (Fig. 4b). At 121.6 nm, the OH(X) rotational distribution peaks at $N = 45$ and OH(X, $v = 0-8$) are observed. Fitting the data indicates that $\sim 75\%$ of the available energy goes into rotational excitation of the OH(X) product, and $\sim 50\%$ of the OH is in $v = 0$. The OH A/X branching ratio is $\sim 20\%$, whereas theory predicts $\sim 30\%$ [15]. In the present study, the OH(X) rotational distribution peaks near $N = 40$, and structure consistent with OH(X) in vibrationally excited states is observed. The OH A/X branching ratio is $< 0.1\%$. Theory predicts a branching ratio of $\sim 10\%$ [11].

The vertical lines in both sets of data in Fig. 4 denote half of the maximum excess energy available to the system. Note that the higher resolution of Harich et al. should be accounted for when comparing the distributions. Namely, with our rotational resolution, their spectrum would peak at $E_{\text{trans}} < 7000 \text{ cm}^{-1}$. The bias towards slow H-atoms (and thus more highly rotationally excited OH product) is less in the present study, i.e., at lower photolysis energies the system exhibits less dynamical bias.

3. Discussion

The absorption of two 266 nm photons excites H_2O to the $\tilde{\text{B}}$ state. Fig. 5 shows slices of the $\tilde{\text{X}}$, $\tilde{\text{A}}$, and $\tilde{\text{B}}$ potential surfaces calculated by van Harrevelt and van Hemert [15]. Unlike the ground state, $\tilde{\text{B}}$ has a linear equilibrium geometry with unequal OH bond lengths of 0.95 and 1.6 Å. The gradients on the $\tilde{\text{B}}$ surface in the Franck–Condon region of the $\tilde{\text{B}} \leftarrow \tilde{\text{X}}$ absorption are greatest in the direction of HOH bending. There is little acceleration along the OH bonds. This accounts for the observation of highly rotationally excited OH with modest vibrational excitation. Conical intersections between $\tilde{\text{B}}$ and $\tilde{\text{X}}$ occur at both the linear HOH ($\theta = 180^\circ$) and the HHO ($\theta = 0^\circ$) geometries. Because $\tilde{\text{A}}$ and $\tilde{\text{B}}$ are a Renner–Teller pair, they are degenerate at linear geometries and can couple via Coriolis interaction.

Following excitation to the $\tilde{\text{B}}$ state via two-photon 266 nm absorption, three possible pathways can yield H-atoms: (i) direct dissociation on $\tilde{\text{B}}$, yielding OH(A) + H; (ii) dissociation via $\tilde{\text{A}}$ following a transition from $\tilde{\text{B}}$ to $\tilde{\text{A}}$; (iii) dissociation on $\tilde{\text{X}}$ following a transition from $\tilde{\text{B}}$ to $\tilde{\text{X}}$, i.e., after passing through the region of conical intersection. Pathways (ii) and (iii) produce OH(X) + H. The OH(A) + H threshold is $\sim 1620 \text{ cm}^{-1}$ below the excitation energy used in the study presented here.

What are the respective roles of these three pathways in the photodissociation dynamics? Experiments

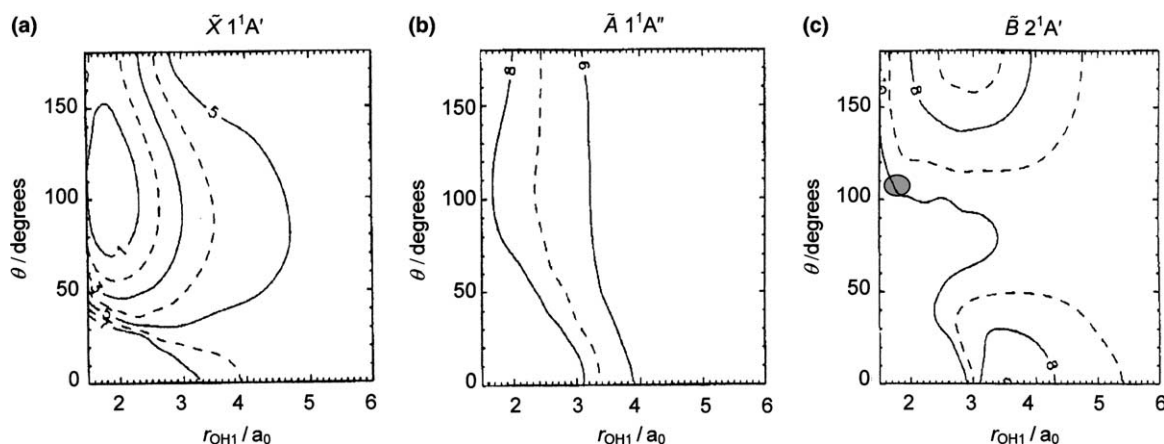


Fig. 5. Slices of the \bar{X} , \bar{A} and \bar{B} surfaces, from [12]. Contours are spaced by 1 eV and $r_{\text{OH}_2} = 0.95 \text{ \AA}$. The \bar{B} state equilibrium is linear with bond lengths of 1.6 and 0.95 \AA . The absorption of two 266 nm photons accesses the \bar{B} state in the Franck–Condon region, indicated by an oval. Bent H_2O moves toward linearity, resulting in highly rotationally excited OH. The \bar{B}/\bar{X} conical intersection results in efficient transfer of flux from \bar{B} to \bar{X} with dissociation occurring on \bar{X} .

with photolysis wavelengths $>125 \text{ nm}$ and sensitivity to both OH(X) and OH(A) have indicated that (i) plays a relatively small role and that the OH(A)+H contribution decreases as the photolysis photon energy decreases [17–19]. For example, fluorescence studies of OH(A) at longer photolysis wavelengths (including $266 \div 2 \text{ nm}$) indicate that OH(A)+H is a minor channel, though it has not been possible to quantify the branching ratio [14,22,24,25]. These studies, combined with our OH A/X branching ratio of $<0.1\%$, indicate that OH(A)+H is indeed a minor channel in the photodissociation dynamics, especially at the longer excitation wavelengths.

The recent theoretical results of van Harrevelt and van Hemert shed light on the importance of \bar{A}/\bar{B} coupling and the \bar{B}/\bar{X} conical intersection in the production of OH(X) [11,15]. They have calculated the \bar{X} , \bar{A} , and \bar{B} potential energy surfaces and transition dipole moment surfaces. They have also calculated the absorption spectrum of cold H_2O and the dissociation dynamics that ensue following $\bar{B} \leftarrow \bar{X}$ photoexcitation.

A wave packet that starts on \bar{B} in the Franck–Condon region at $t = 0$ develops flux on \bar{X} within 2 fs. Within 10 fs the center of the packet has reached the linear HOH region. From there the packet bifurcates, with parts proceeding on \bar{X} and \bar{B} . Dissociation on \bar{X} occurs quickly, beginning at $\sim 25 \text{ fs}$, which leaves little time for highly excited bending motion in H_2O to redistribute among other vibrational degrees of freedom. This results in highly rotationally excited OH(X). Dissociation on \bar{B} begins at $\sim 25 \text{ fs}$ as well, and results in rotationally excited OH(A), with a distribution that peaks near the largest N value that is energetically allowed. Little flux develops on \bar{A} indicating the relative unimportance of \bar{A}/\bar{B} coupling, at least for rotationally cold molecules.

The main result of this article – the lack of any discernible signal arising from the OH(A)+H channel – is unequivocal. The HRTOF method gives accurate values for relative H-atom yields, and the traces shown in the insert in Fig. 3 enable us to place confidently an upper bound of 0.1% on the A/X branching ratio. As product energies are known with good accuracy, the excess energy of 1620 cm^{-1} is also reliable, say to $\pm 30 \text{ cm}^{-1}$ [26].

In plain terms, the wave packet evolves to the region of the HOH conical intersection (and conceivably toward the O+H₂ channels) with essentially 100% efficiency. No flux appears in the OH(A)+H channel. The initial momentum distribution is not so prejudiced against the OH(A)+H pathway as to account for this observation by itself. Rather, the shape of the potential in the Franck–Condon region must account for the large bias. Therefore, we conclude that in the Franck–Condon region gradients in the r_{OH} coordinate are smaller than predicted theoretically. Referring to Fig. 5, the gradients in the Franck–Condon region direct the wave packet toward a sharply downhill region of the potential that leads to the conical intersection.

Acknowledgements

This research was supported by the US Department of Energy, Office of Basic Energy Sciences, under Grant number DE-FG02-04ER15509.

References

- [1] D.W. Hwang, X. Yang, X. Yang, *J. Chem. Phys.* 110 (1999) 4119.
- [2] V. Engel, V. Staemmler, R.L. Vander Wal, F.F. Crim, R.J. Sension, B. Hudson, P. Andresen, S. Hennig, K. Weide, R. Schinke, *J. Phys. Chem.* 96 (1992) 3201.

- [3] T. Schröder, R. Schinke, M. Ehara, K. Yamashita, *J. Chem. Phys.* 109 (1998) 6641.
- [4] D.F. Plusquellic, O. Votava, D.J. Nesbitt, *J. Chem. Phys.* 107 (1997) 6123.
- [5] D.F. Plusquellic, O. Votava, D.J. Nesbitt, *J. Chem. Phys.* 109 (1998) 6631.
- [6] O. Votava, D.F. Plusquellic, D.J. Nesbitt, *J. Chem. Phys.* 110 (1999) 8564.
- [7] M. Brouard, S.R. Langford, D.E. Manolopoulos, *J. Chem. Phys.* 101 (1994) 7458.
- [8] K. Weide, K. Kühn, R. Schinke, *J. Chem. Phys.* 91 (1989) 3999.
- [9] K. Weide, R. Schinke, *J. Phys. Chem.* 90 (1989) 7150.
- [10] M. von Dirke, B. Heumann, K. Kühn, T. Schröder, R. Schinke, *J. Chem. Phys.* 101 (1994) 2051.
- [11] R. van Harrevelt, M.C. van Hemert, *J. Chem. Phys.* 112 (2000) 5787.
- [12] K. Weide, R. Schinke, *J. Chem. Phys.* 87 (1987) 4627.
- [13] B. Heumann, K. Kühn, K. Weide, R. Düren, B. Hess, U. Meier, S.D. Peyerimhoff, *Chem. Phys. Lett.* 166 (1990) 385.
- [14] J.H. Fillion, R. van Harrevelt, J. Ruiz, M. Castillejo, A.H. Zanganeh, J.L. Lemaire, M.C. van Hemert, F. Rostas, *J. Phys. Chem. A* 105 (2001) 1141.
- [15] R. van Harrevelt, M.C. van Hemert, *J. Chem. Phys.* 112 (2000) 5777.
- [16] D. Yarkony, *Mol. Phys.* 93 (1998) 971.
- [17] H.J. Krautwald, L. Schnieder, K.H. Welge, M.N.R. Ashfold, *Faraday Discuss. Chem. Soc.* 82 (1986) 99.
- [18] D.H. Mourdaunt, M.N.R. Ashfold, R.N. Dixon, *J. Chem. Phys.* 100 (1994) 7360.
- [19] S.A. Harich, D.W.H. Hwang, X. Yang, J.J. Lin, X. Yang, R.N. Dixon, *J. Chem. Phys.* 113 (2000) 10073.
- [20] J. Zhang, M. Dulligan, C. Wittig, *J. Phys. Chem.* 99 (1995) 7446.
- [21] T. Carrington, *J. Chem. Phys.* 41 (1964) 2012.
- [22] J.P. Simons, A.J. Smith, R.N. Dixon, *J. Chem. Soc. Faraday Trans. 2* (80) (1984) 1489.
- [23] A. Hodgson, J.P. Simons, M.N.R. Ashfold, J.M. Bayley, R.N. Dixon, *Mol. Phys.* 54 (1985) 351.
- [24] N. Shafizadeh, J. Rostas, J.L. Lemaire, F. Rostas, *Chem. Phys. Lett.* 152 (1988) 75.
- [25] C.G. Atkins, R.G. Briggs, J.B. Halpern, G. Hancock, *Chem. Phys. Lett.* 152 (1988) 81.
- [26] B. Ruscic, A.F. Wagner, L.B. Harding, R.L. Asher, D. Feller, D.A. Dixon, K.A. Peterson, Y. Song, X. Qian, C.-Y. Ng, J. Liu, W. Chen, D.W. Schwenke, *J. Phys. Chem. A* 106 (2002) 2727.
- [27] J.A. Coxon, *Canadian J. Phys.* 58 (1980) 933.
- [28] C.E. Moore, *Atomic Energy Levels*, National Bureau of Standards, Washington, DC, 1949.
- [29] K. Watanabe, M. Zelikoff, *J. Opt. Soc. Am.* 43 (1953) 753.